Structure of the dinuclear rhodium complex (Cp*Rh)2(CH3)2(.mu.-CH2)2 and the CC coupling reaction of its model complexes. An ab initio MO study

Nobuaki. Koga, and Keiji. Morokuma

Organometallics, **1991**, 10 (4), 946-954• DOI: 10.1021/om00050a028 • Publication Date (Web): 01 May 2002

$C_{27}H_{35}BF_5PSn$ (615.0): C, 52.7; H, 5.74. Found: C, 52.82; H, 5.82.

(ii) Reaction of 4 with BF_3·OEt_2 in the Presence of Benzophenone. The white residue is treated with 20 mL of chloroform as above and filtered, and the filtrate is evaporated to dryness. A 10-mL aliquot of THF is added, and after 2 days, colorless crystals of the vinylphosphonium salt **15** have precipitated.

(2,2-Diphenylvinyl)triphenylphosphonium Tetrafluoroborate (15). Yield: 1.02 g (55%). Mp: 199–201 °C. ^{1}H NMR ($CDCl_3$): δ = 6.67–7.09 (m, 5 H, aromatic H), 7.37 (s (broad), 5 H, aromatic H), 7.51–7.59 (m, 15 H, aromatic H). ^{31}P NMR ($CDCl_3$): δ = 9.9 (s, PPh_3). ^{11}B NMR ($CDCl_3$): δ = −0.85 (s (sharp), BF_4).

(iii) Reaction of 5 with BF_3·OEt_2. The reaction is performed and worked up as described above. The colorless remaining foam is crystallized from 5 mL of toluene and 10 mL of diethyl ether.

1-(Di-*tert*-butylfluorostannyl)-1-(trifluoroborato)-1-(triphenylphosphonio)ethane (22). Yield: 1.72 g (81%). ^{1}H NMR ($CDCl_3$): δ = 0.86 (s, 9 H, tBu CH_3, $J_{^{119}SnH}$ = 99.1 Hz, $J_{^{117}SnH}$ = 95.2 Hz), 1.37 (s, 9 H, $tBuCH_3$, $J_{^{119}SnH}$ = 85.0 Hz, $J_{^{117}SnH}$ = 82.0 Hz), 1.84 (d, J_{PH} = 22.7 Hz, 3 H, CH_3), 7.37–8.01 (m, 15 H, aromatic H). ^{19}F NMR ($CDCl_3$): δ = −124.8 (m, 3 F, BF_3), −186.8 (s, 1 F, SnF, $J_{^{119}SnF}$ = 2573 Hz, $J_{^{117}SnF}$ = 2463 Hz). ^{11}B NMR ($CDCl_3$): δ = 4.16 (s, $\nu_{1/2}$ = 180 Hz).

(iv) Reaction of 5 with BF_3·OEt_2 in the Presence of Benzophenone. The colorless solid is recrystallized from 5 mL of THF. Diphenylcarbinol (**24**) can be detected by NMR spectroscopy or GC/MS after the diethyl ether used for washing was shaken with 10% sodium carbonate.

1-(Di-*tert*-butylfluorostannyl)vinyltriphenylphosphonium Tetrafluoroborate (23). Yield: 1.53 g (70%). Mp: 191–192 °C. ^{1}H NMR ($CDCl_3$): δ = 1.17 (d, J_{HF} = 1.5 Hz, 18 H, $tBuCH_3$, $J_{^{119}SnH}$ = 100.83 Hz, $J_{^{117}SnH}$ = 96.19 Hz), 6.93 [d (the geminal coupling constant J_{HH} could not be resolved), J_{PH} = 37.35 Hz, 1 H, vinyl CH_2], 6.99 [d (the geminal coupling constant J_{HH} could not be resolved), J_{PH} = 35.64 Hz, 1 H, vinyl CH_2], 7.63–7.90 (m, 15 H, aromatic H). ^{19}F NMR ($CDCl_3$): δ = −150.4 (s, 4 F, BF_4), −196.5 (s, 1 F, SnF, $J_{^{119}SnF}$ = 2448 Hz, $J_{^{117}SnF}$ = 2338 Hz). ^{11}B NMR ($CDCl_3$): δ = −0.84 (s (sharp), BF_4). Anal. Calcd for $C_{28}H_{35}BF_5PSn$ (627.1): C, 53.63; H, 5.63. Found: C, 53.61; H, 5.68.

(v) Reaction of 9 with BF_3·OEt_2. Attempts to recrystallize crude **27** lead to decomposition.

{1,3,7,9-Tetra-*tert*-butyl-2,2,8,8-tetramethyl-5,10-bis(triphenylphosphonio)-1,3,7,9-tetraaza-2,8-disila-4,6-distannadispiro[3.3.3]decane} Bis(tetrafluoroborate) (27). ^{1}H NMR (CD_3CN): δ = −0.11 (s, 12 H, CH_3), 0.77 (s, 36 H, $tBuCH_3$), 3.72 (d, J_{PH} = 19.5 Hz, 2 H, CH), 7.36–7.77 (m, 30 H, aromatic H). ^{11}B NMR (CD_3CN): δ = 4.25 (s (sharp), BF_4).

Di[1,3-di-tert-butyl-4-(triphenylphosphoranylidene)-methyl-2,2-dimethyl-1,3,2,4-diazasilastannetyl] (28). A 2-g (1.5 mmol) sample of **23** is dissolved in 10 mL of acetonitrile, and 1.2 g (3 mmol) of methyltriphenylphosphonium iodide is added. Instantaneously, the reaction mixture turns violet, and at −30 °C 1.26 g (71%) of **28** crystallizes slowly; mp 198–200 °C. The compound is only sparingly soluble in common solvents. ^{1}H NMR (CD_2Cl_2): δ = 0.08 (s, 6 H, CH_3), 0.24 (s, 6 H, CH_3), 1.08 (s, 36 H, tBu CH_3), 1.23 (d, J_{PH} = 4.4 Hz, 2 H, CH), 7.40–7.86 (m, 30 H, aromatic H). ^{31}P NMR (CD_2Cl_2): δ = 20.21 (s, $J_{^{119}SnP}$ = 180.9 Hz, $J_{^{117}SnP}$ = 172.8 Hz). MS (field desorption, 6.5 kV): m/z 1187 [M (^{119}Sn), 100%]. Anal. Calcd for $C_{58}H_{80}N_4P_2Si_2Sn_2$ (1188.84): C, 58.59; H, 6.78. Found: C, 58.62; H, 6.74.

Acknowledgment. This work was supported by Prof. W. Sundermeyer, Prof. G. Huttner, the Deutsche Forschungsgemeinschaft, and the Fonds der Chemischen Industrie. We thank Prof. W. W. Schoeller for fruitful discussions and S. Pitter for the GC/MS investigation.

Supplementary Material Available: Tables of atomic and thermal parameters and bond lengths and angles for **11**, **12**, and **23** (11 pages); listings of structure factors for **11**, **12**, and **23** (33 pages). Ordering information is given on any current masthead page.

Structure of the Dinuclear Complex $(Cp^*Rh)_2(CH_3)_2(\mu\text{-}CH_2)_2$ and the CC Coupling Reaction of Its Model Complexes. An ab Initio MO Study

Nobuaki Koga and Keiji Morokuma*

Institute for Molecular Science, Myodaiji, Okazaki 444, Japan

Received October 1, 1990

The structure of $(Cp^*Rh)_2(\mu\text{-}CH_2)_2(CH_3)_2$ (**1**) has been studied with an ab initio MO method using the model complex $(CpRh)_2(\mu\text{-}CH_2)_2(CH_3)_2$ (**2**). The calculated geometry of **2** agrees well with that of **1** determined experimentally. A theoretical analysis shows that there is a Rh d–Rh d σ bond and that the Rh–CH_2 bonds are strained. We have also studied the CC coupling reaction, in which the structure and the energetics of the model reactant $(CpRh)_2(\mu\text{-}CH_2)_2(CH_3)(H)$ (**3**), the product $(CpRh)_2(\mu\text{-}CH_2)(C_2H_5)(H)$ (**4**), and the transition state connecting them have been determined theoretically. The reaction proceeds via a reductive elimination and not via a dinuclear replacement. At the best (RMP2) level of calculation the reaction has an activation energy of 42 kcal/mol and is endothermic by 25 kcal/mol. This reductive elimination reaction of the dinuclear complex **3** is easier than that of the mononuclear complex $CpRh(PH_3)(CH_3)_2$. In the former the strain in the Rh–CH_2 bonds and the positive charge on CH_2, in contrast to negative on CH_3, lower the activation energy.

Introduction

For the Fischer–Tropsch synthesis,[1] several mechanisms have been so far proposed.[2-7] Scheme I shows the

Scheme I

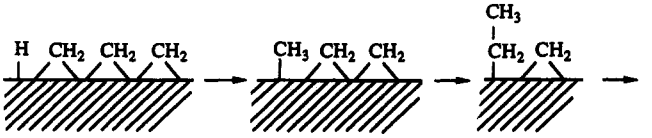

mechanism proposed by Brady and Pettit,[2] which is a modification of Fischer and Tropsch's original proposal.[3]

(1) (a) Rofer-DePoorter, C. K. *Chem. Rev.* **1981**, *81*, 447. (b) Herrmann, W. A. *Angew. Chem., Int. Ed. Engl.* **1982**, *21*, 117.
(2) Brady, R. C.; Pettit, R. *J. Am. Chem. Soc.* **1980**, *102*, 6181.
(3) (a) Fischer, F.; Tropsch, H. *Brennst.-Chem.* **1926**, *7*, 97. (b) Fischer, F.; Tropsch, H. *Chem. Ber.* **1926**, *59*, 830.
(4) Biloven, P.; Helle, H. N.; Sachtler, W. M. H. *J. Catal.* **1979**, *58*, 95.

0276-7333/91/2310-0946$02.50/0

In this mechanism a hydrogen on the surface inserts into a surface–CH_2 bond to form a methyl group. In the chain-propagation step the alkyl group thus generated inserts into a surface–CH_2 bond. In order to shed light on the mechanism of the Fischer–Tropsch synthesis, model reactions of transition-metal complexes have been studied.[1b] Among those studied, recent experiments on thermal decomposition of the dinuclear Rh complex $(Cp^*Rh)_2(\mu\text{-}CH_2)_2(CH_3)_2$ (1), where $Cp^* = C_5(CH_3)_5$, have drawn substantial attention (eq 1).[8] One of the main products is

$$(Cp^*Rh)_2(\mu\text{-}CH_2)_2(CH_3)_2 \xrightarrow{\Delta} CH_4 + C_3H_6 + C_2H_4 + \ldots \quad (1)$$

propene, and the isotope experiments have revealed that this is formed through CC coupling between CH_3 and the bridging CH_2. This is speculated to correspond to a key reaction in Scheme I.

In this paper, we report the results of ab initio MO calculations on the structure of $(CpRh)_2(\mu\text{-}CH_2)_2(CH_3)_2$ (2),

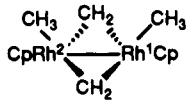

2

where Cp = cyclopentadienyl, C_5H_5, which is a model complex of 1, and on the CC coupling reaction of $(CpRh)_2(\mu\text{-}CH_2)_2(CH_3)$ (H) (3) in which the nonreacting CH_3 of 2 is replaced by H to save CPU time (eq 2). We

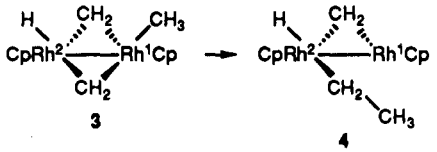

(2)

determined the structure of the transition state as well as those of the reactant and the product by the ab initio restricted Hartree–Fock (RHF) molecular orbital (MO) method with the energy gradient technique. Although we have studied several elementary organometallic reactions and a few full catalytic cycles with such a method,[9,10] this is the first time the method has been applied to a reaction of such a large dinuclear complex.

In addition, we compared the energetics of the CC coupling reaction of the model Rh dinuclear complex (eq 2) with that of the ethane reductive elimination reaction of a Rh mononuclear complex (eq 3), in order to clarify the reason that the CC coupling reaction can take place

$$\underset{5}{CpRh(PH_3)(CH_3)_2} \rightarrow \underset{6}{CpRh(Ph_3)(C_2H_6)} \rightarrow CpRh(PH_3) + C_2H_6 \quad (3)$$

$$\underset{7}{}$$

relatively easily in the dinuclear complex, so that it is regarded as a model reaction for the Fischer–Tropsch synthesis. The reductive elimination of two alkyl groups from a similar Pt complex $CpPt(CH_3)_3$ is known not to take place.[11] A high activation barrier of ethane reductive elimination from $M(CH_3)_2(PH_3)_2$ (M = Pd, Pt) has been found also by theoretical calculations.[12]

In this paper, after a short description of the computational method in the second section, we will present in the third section the results and discussion on the structure of the model complex 2. The results for reactions 2 and 3 will be presented in the fourth and fifth sections, respectively. The comparison between reactions 2 and 3 is made in the sixth section. The seventh section contains concluding remarks.

Computational Method

All the transition-state structures as well as the equilibrium structures were optimized by using the ab initio RHF MO energy gradient method[13] with a relativistic effective core potential (ECP)[14a] and valence double-ζ basis functions[14a] for Rh and the STO-2G basis functions[15a] for all the ligands. The number of valence electrons of Rh taken into account explicitly is 9. This basis set is denoted as I in this paper. This basis set used for the geometry optimization is rather poor. As shown in the following sections, however, this small basis set yields for reaction 3 structures very similar to those obtained with a larger basis set in which the 3-21G basis functions[15b] are adopted for the active ligands, CH_3, CH_2, and the hydride, and the STO-2G for the spectator ligands, PH_3 and Cp (this basis set is denoted as II). We have been using basis set II for the structure determination of several elementary organometallic reactions and catalytic cycles to obtain reasonable results.[9,10]

In the structure determination we assumed a C_{2v} symmetry for 2 and a C_s symmetry for 3, 5–7, and the transition state between 5 and 6. The structure of the Cp ligand in 2 was determined with the restriction of local C_{5v} symmetry; the averaged C–H and C–C distances and the H–C–X (center of the C_{5v} Cp ring) bending angle were optimized. The local Cp structures in 4 and the transition state between 3 and 4 was taken from that of 2 thus determined, and the rotation of Cp rings around Rh–X axis was frozen at 0° for one of the RhRhXC dihedral angles, whereas the distance, the angle, and the dihedral angle on which the position of X depends could change during the structure determination. In the case of 5–7 and the transition state between 5 and 6, the structure of the Cp ring was determined with restriction of the local C_{5v} symmetry. The effect of this restriction on the structures and energetics for reaction 3 was investigated and will be shown later. In short, such a restriction changes the energetics by only 2–3 kcal/mol.

In order to include electron correlation effects for more reliable energetics, we carried out the frozen-core Møller–Plesset second-order perturbation (MP2) calculations. In these calculations a larger basis set denoted as III was used: 6-31G* for CH_3, CH_2,

(5) (a) Storch, H. H.; Golumbic, N.; Anderson, R. B. *The Fischer-Tropsch and Related Synthesis*; Wiley: New York, 1951. (b) Kummer, J. F.; Emmett, P. H. *J. Am. Chem. Soc.* **1953**, *75*, 5177.

(6) Pichler, H.; Schultz, H. *Chem. Eng. Tech.* **1970**, *12*, 1160.

(7) (a) Masters, C. *Adv. Organomet. Chem.* **1979**, *17*, 61. (b) Henrici-Olivé, G.; Olivé, S. *Angew. Chem., Int. Ed. Engl.* **1976**, *15*, 136. (c) McCandlish, L. E. *J. Catal.* **1983**, *83*, 362.

(8) (a) Isobe, K.; Andrews, D. G.; Mann, B. E.; Maitlis, P. M. *J. Chem. Soc., Chem. Commun.* **1981**, 809. (b) Isobe, K.; Varzquez de Miguel, A.; Bailey, P. M.; Okeya, S.; Maitlis, P. M. *J. Chem. Soc., Dalton Trans.* **1983**, 1441. (c) Saez, I. M.; Meanwell, N. J.; Nutton, A.; Isobe, K.; Varzquez de Miguel, A.; Bruce, D. W.; Okeya, S.; Andrews, D. G.; Ashton, P. R.; Johnstone, I. R.; Maitlis, P. M. *J. Chem. Soc., Dalton Trans.* **1986**, 1565.

(9) (a) Obara, S.; Kitaura, K.; Morokuma, K. *J. Am. Chem. Soc.* **1984**, *106*, 7482. (b) Koga, N.; Obara, S.; Kitaura, K.; Morokuma, K. *J. Am. Chem. Soc.* **1985**, *107*, 7109. (c) Koga, N.; Morokuma, K. *J. Am. Chem. Soc.* **1986**, *108*, 6136. (d) Koga, N.; Jin, S.-Q.; Morokuma, K. *J. Am. Chem. Soc.* **1988**, *110*, 3417. (e) Nakamura, S.; Morokuma, K. *Organometallics* **1988**, *7*, 1904. (f) Koga, N.; Morokuma, K. *J. Phys. Chem.* **1990**, *94*, 5454. (g) Maseras, F.; Koga, N.; Morokuma, K. To be published. (h) Kawamura, H.; Koga, N.; Morokuma, K. To be published.

(10) (a) Daniel, C.; Koga, N.; Han, J.; Fu, X.-Y.; Morokuma, K. *J. Am. Chem. Soc.* **1988**, *110*, 3773. (b) Ding, Y.-B.; Koga, N.; Jin, S.-Q.; Morokuma, K. Unpublished result.

(11) Egger, K. W. *J. Organomet. Chem.* **1970**, *24*, 501.

(12) (a) Low, J. J.; Goddard, W. A., III *J. Am. Chem. Soc.* **1984**, *106*, 6928. (b) Low, J. J.; Goddard, W. A., III *J. Am. Chem. Soc.* **1984**, *106*, 8321.

(13) We used the GAUSSIAN82 program,[13a] in which the ECP codes are implemented.[13b,c] (a) Binkley, J. S.; Frisch, M. J.; DeFrees, D. J.; Raghavachari, K.; Whiteside, R. A.; Schlegel, H. B.; Pople, J. A. Carnegie-Mellon Chemistry Publishing unit, Pittsburgh, PA, 1984. (b) McMurchie, L. E.; Davidson, E. R. *J. Comput. Phys.* **1981**, *44*, 289. (c) Martin, R. L. Unpublished results.

(14) (a) Hay, P. J.; Wadt, W. R. *J. Chem. Phys.* **1985**, *82*, 270. (b) Hay, P. J.; Wadt, W. R. *J. Chem. Phys.* **1985**, *82*, 299.

(15) (a) Hehre, W. J.; Stewart, R. F.; Pople, J. A. *J. Chem. Phys* **1969**, *51*, 2657. (b) Binkley, J. S.; Pople, J. A.; Hehre, W. J. *J. Am. Chem. Soc.* **1980**, *102*, 939. (c) Hehre, W. J.; Ditchfield, R.; Pople, J. A. *J. Chem. Phys.* **1972**, *56*, 2257. Hariharan, P. C.; Pople, J. A. *Theor. Chim. Acta* **1973**, *28*, 213.

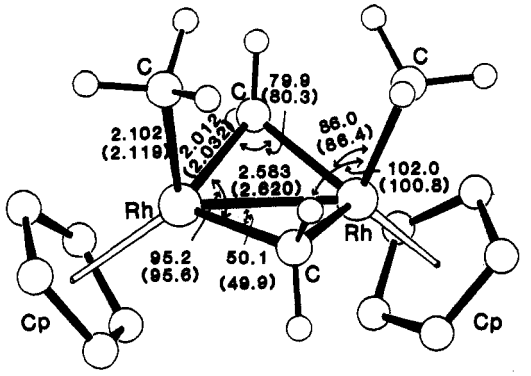

Figure 1. RHF/I-optimized structure in angstroms and degrees of $(CpRh)_2(\mu\text{-}CH_2)_2(CH_3)_2$ (2) with the constraint of an overall C_{2v} symmetry and a local C_{5v} symmetry for Cp. Numbers in parentheses are experimental values of 1. Hydrogen atoms of Cp's are omitted for clarity.

and the hydride and STO-3G for the Cp rings,[15a,c] with the same ECP and valence basis functions for Rh. We do not use the f polarization function on Rh. The effect of this polarization function in Rh_2 has been found to be small.[16]

The present ECP is more attractive than the ECP with 17 valence electrons[14b] at the RHF level.[9f,g] This difference is not as large as the energy difference between reactions 2 and 3, and the results obtained with the two ECPs are qualitatively similar at the correlated level.[9f,g] The main purpose of this paper is not to reproduce the energetics of the reaction accurately but to compare the reactions between the di- and mononuclear complexes qualitatively, as seen in the use of poor STO-2G basis functions in set I and II. For comparison we also carried out some energy calculations with the 17 valence electron ECP with the [3s3p2d] basis functions for Rh,[14b] 3-21G for the active ligands, and STO-2G for the spectator ligands (basis set IV).

Results and Discussion

Structure of Model Complex $(CpRh)_2(\mu\text{-}CH_2)_2(CH_3)_2$ (2): Rh–Rh and Rh–CH_2 Bonds. The optimized structure of $(CpRh)_2(\mu\text{-}CH_2)_2(CH_3)_2$ (2) shown in Figure 1 is in good agreement with the experimental structure of 1 determined by the X-ray experiment, although the basis set I used here is the smallest. The difference between theory and experiment is 0.04 Å for the Rh–Rh bond distance and 0.02 Å for the Rh–CH_2 and Rh–CH_3 bond lengths. As to the bond angles, the agreement is better; the differences in the Rh–C–Rh and the C–Rh–C angles are less than 1°. The distance between the Rh atoms and the carbons of the Cp rings is calculated to be 2.279 Å, whereas the experimental mean Rh–C distance is 2.272–2.291 Å.

Of particular interest in 2 are the Rh–Rh and the bridged Rh–CH_2–Rh bonds. The Rh–Rh bond is expected to exist, since Rh atoms have a formal electron count of d^5 and the unpaired d electron of each Rh could form a Rh–Rh bond. Experimentally, complex 1 is diamagnetic.[8b] In order to investigate these bonds, we calculated the Boys-localized molecular orbitals (LMOs).[17] Those representing the Rh–Rh and the Rh–CH_2 bonds are shown in Figure 2a,b. One can clearly see the Rh–Rh σ bond consisting mainly of the d_{y^2} orbital of each Rh atom. This LMO delocalizes the Rh–CH_2 bond region slightly, since the Rh–CH_2 bonds are in the vicinity of the Rh–Rh bond.

To explain the Rh–Rh σ bond, we considered the interaction between the singly occupied orbitals of the $CpRh(CH_3)_3$ (8) fragments with the formal electron count of d^5. In Figure 3 is shown the orbital interaction diagram.

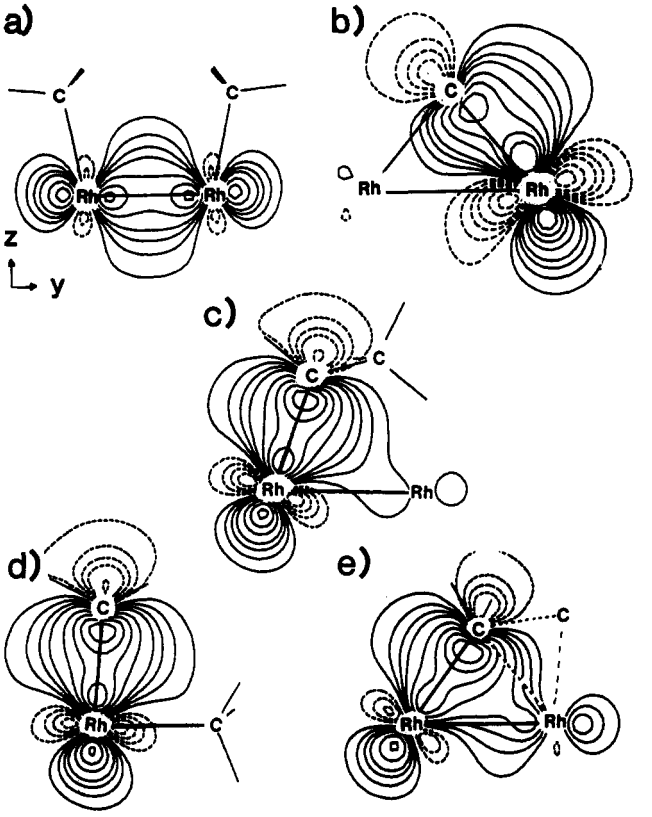

Figure 2. Boys-localized molecular orbitals of 2 for (a) the Rh–Rh bond and (b) a Rh–CH_2 bond and those for (c) a Rh–C_2H_5 bond of 4, (d) a Rh–CH_3 bond of 5, and (e) a Rh–CH_2(···CH_3) bond of the transition state between 3 and 4. The contours are ±0.3, ±0.25, ±0.2, ±0.15, ±0.1, ±0.075, ±0.05, and ±0.025 au, and solid and dotted lines denote positive and negative values, respectively.

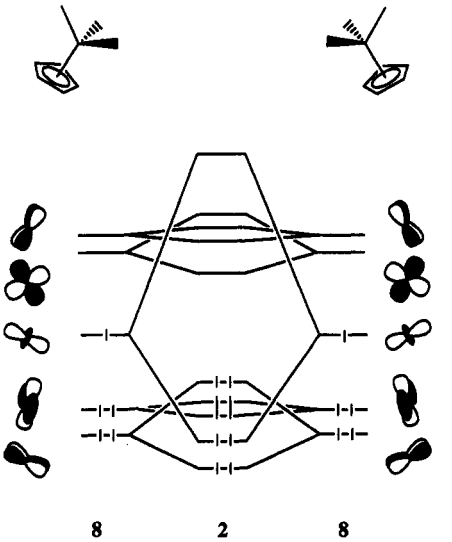

Figure 3. Schematic orbital interaction diagram for $(CpRh)_2(\mu\text{-}CH_2)_2(CH_3)_2$.

On both sides of Figure 3, the d-orbital energy levels of 8 are shown. It is well-known that the Cp ring can be replaced by three carbonyl ligands, when the electronic structure is qualitatively discussed.[18] Therefore, the d energy levels of d^6 $[CpRh(CH_3)_3]^-$, anion of 8, would be similar to the levels of familiar six-coordinate d^6 complexes with the occupied t_{2g} and the vacant e_g orbitals. This anionic species, $[CpRh(CH_3)_3]^-$, is isoelectronic to 5. For

(16) Das, K. K.; Balasubramanian, K. *J. Chem. Phys.* **1990**, *93*, 625.
(17) Boys, S. F. In *Quantum theory of atoms, molecules and the Solid State*; Löwdin, P.-O, Ed.; Academic Press: New York, 1968.
(18) Albright, T. A.; Burdett, J. K.; Whangbo, M.-H. *Orbital Interactions in Chemistry*; Wiley: New York, 1985; p 387.

8 having a formal electron count of d^5, the singly occupied d orbital is located at the center of the d levels and is responsible for the Rh–Rh σ bond.

The Rh–CH_2 bond orbital in Figure 2b is slightly deformed; its centroid deviates from the line connecting Rh and C. This suggests a strain in the Rh–CH_2 bond due to the small Rh–C–Rh angle of 80°. In this regard, the LMO of the Rh–CH_2 bond is very different from the LMO representing the Rh–CH_3 bond in **5** shown in Figure 2d, in which no strain is expected, and thus its centroid is located on the line connecting Rh and C. The Rh–CH_2 bond, which is shorter than the Rh–CH_3 bond, is similar to the cyclopropane C–C bond (1.491 (6-31G*) and 1.510 Å (experiment[19a])), which, with a substantial strain, is shorter than the ethane C–C bond (1.527 (6-31G*) and 1.532 Å (experiment[19b])). This strain also destabilizes the carbon orbitals, while the small Rh–Rh–C angle of 50° does not affect the Rh d orbital in bonding, since the angle between two d orbitals, say, d_{xy} and $d_{x^2-y^2}$, is 45°. Therefore, the weight of the carbon orbitals in the Rh–CH_2 LMO is smaller than that in the Rh–CH_3 LMO as seen in Figure 2. One can say the μ-CH_2 group is more electropositive than the CH_3 group. The Mulliken population analysis at the RHF/I level shows that the μ-CH_2 and the CH_3 groups have positive charges of +0.2605 and +0.1299, respectively, and thus the μ-CH_2 group is more positive by 0.13 e than the CH_3 group. At the RHF/I level, because of the basis set superposition error, the absolute value of the charges is not reliable, though the difference is meaningful. The changes in **3** calculated at the RHF/III level will be discussed later. The more positive μ-CH_2 is in accord with the experimental facts that the ^1H and ^{13}C signals for μ-CH_2 are observed in the low-field region ($\delta(^1H)$ = 6–10 and $\delta(^{13}C)$ = 100–190).[8,20,21]

A larger Rh–C–Rh angle would release this strain but would cause repulsion between the Rh–CH_2 bonds and the Rh–Rh σ bond. The small angle of 80° presumably keeps CH_2 groups away from the Rh–Rh bond to reduce this repulsion and further to keep the Rh–Rh bond length within the range of a Rh–Rh single bond, though this imposes strain on the RhCRh triangles.

CC Coupling Reaction in the Dinuclear Complex. The above results demonstrate that the present basis set I gives an acceptable structure model. Energy calculations with better basis sets of the structures determined with this small basis set are expected to be reasonable. Accordingly, using the small basis set I, we studied reaction 2, the reductive elimination of CH_3 and μ-CH_2 from one of the Rh atoms (Rh^1), in which the two Rh^1–ligand bonds are broken and a C–C bond is formed. The reaction results in the reduction of Rh^1 from the formal electron count of d^5 to d^7. The optimized structures for **3**, **4**, and the transition state between them are shown in Figure 4.

Upon the replacement of CH_3 by H on Rh^2 the structure of the complex changes little; from the structure of **2** to that of **3**, the Rh–Rh distance decreases by only 0.008 Å and the Rh–CH_2 distances increase by 0.004 and 0.008 Å. Thus, this replacement, the purpose of which is to save the computational time, is expected not to change the chemistry of the CC coupling reaction.

The geometry optimization of product **4** gave the Rh–Rh distance of 2.624 Å, similar to that in **3**. In **4**, the Rh–Rh

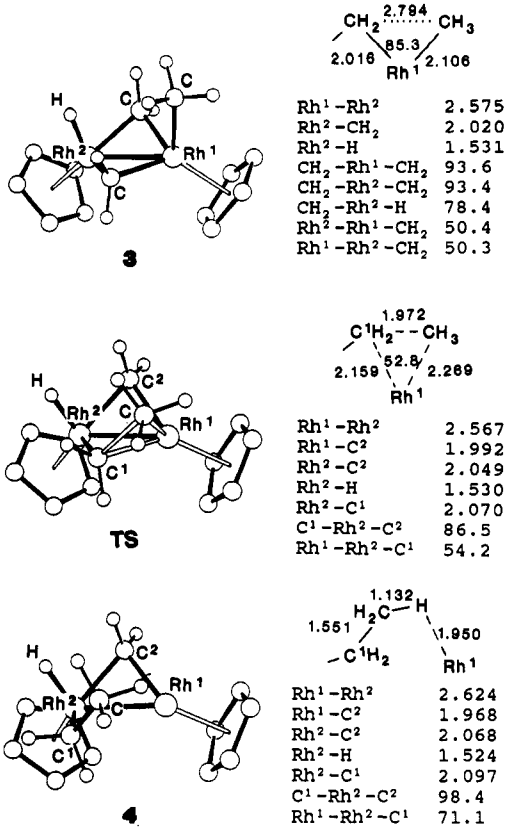

Figure 4. RHF/I-optimized structures in angstroms and degrees of $(CpRh)_2(\mu\text{-}CH_2)_2(CH_3)(H)$ (**3**), $(CpRh)_2(\mu\text{-}CH_2)(C_2H_5)(H)$ (**4**), and the transition state between them, with the structure of Cp fixed to that of **2** and the constraint of an overall C_s symmetry for **3**.

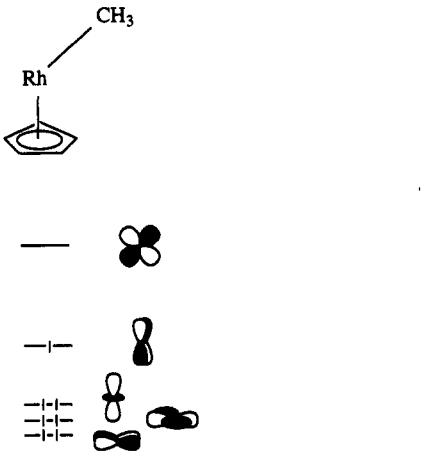

Figure 5. Schematic orbital energy diagram for d^7 $CpRh(CH_3)$.

bond is formed by the singly occupied d orbitals of d^7 Rh^1 and d^5 Rh^2. The orbital energy level of d^7 $CpRh(CH_3)$ is shown in Figure 5. The closed-shell state of CpRhL with the formal electron count of d^8 has four occupied orbitals and one vacant d orbital, from which the removal of one d electron results in one singly occupied and one vacant d orbital. Throughout the course of reaction one of the RhCRh triangles is retained, whose structure remained similar to that in **3**. The other triangle is broken as the result of the reaction, and thus, the C–Rh–Rh angle increases; the CH_2–Rh–Rh angle in **3** is 50.3°, while the C_2H_5–Rh–Rh angle in **4** is 71.1°. This difference suggests that the strain in the Rh–CH_2 bond is released during the reaction, as seen in the LMOs for the Rh–C_2H_5 bond (Figure 2c) and for the Rh–CH_2 bond (Figure 2b).

(19) (a) Butcher, R. J.; Jones, W. J. *J. Mol. Spectrosc.* **1973**, *47*, 64. Jones, W. J.; Stoicheff, B. P. *Can. J. Phys.* **1964**, *42*, 2259. (b) Iijima, T. *Bull. Chem. Soc. Jpn.* **1972**, *45*, 1291.

(20) Herrmann, W. A. *Angew. Chem., Int. Ed. Engl.* **1978**, *17*, 800 and references cited therein.

(21) Herrmann, W. A.; Plank, J.; Riedel, D.; Ziegler, M. L.; Weidenhammer, K.; Guggolz, E.; Balbach, B. *J. Am. Chem. Soc.* **1981**, *103*, 63.

Table I. Energies (in kcal/mol) for the Reaction $(CpRh)_2(\mu\text{-}CH_2)_2(CH_3)(H) \rightarrow (CpRh)_2(\mu\text{-}CH_2)(C_2H_5)(H)$, Relative to the Reactant and Calculated for the RHF/I-Optimized Structures

method	reactant[a]	transition state	product
RHF/I	-526.5942	23.1	-3.6
RHF/II	-530.6642	19.6	-7.9
RHF/III	-542.3532	21.7	-9.0
RMP2/III	-543.8458	41.8	24.9
RHF/IV	-703.6624	27.5	-15.3

[a] Total energies in hartree.

Since the vacant coordination site where the vacant d orbital extends is located on Rh^1, the electron donative interaction from a β-CH bond of C_2H_5 to d^7 Rh^1 can take place in 4. One can see in Figure 4 a long β-CH bond of 1.132 Å and the short H···Rh^1 distance of 1.950 Å, indicating the existence of a strong agostic interaction[22] between β-CH of the ethyl group and the d^7 Rh^1 atom. It has been stated experimentally[23] and theoretically[24] that the origin of the agostic interaction is the donative interaction. In some polynuclear complexes, such an agostic interaction between a transition metal and an alkyl ligand attached to another metal center has been observed experimentally.[22,25]

As shown in the Appendix, the ground state of d^8 CpRhL is not a closed-shell singlet but a triplet, in which the two highest d orbitals are singly occupied. In 4, accordingly, Rh^1 may have a triplet electronic structure, since $CpRh^1(CH_2)$ is isolobal to CpRhL. However, the above-mentioned agostic interaction would push up the vacant orbital in energy, thus making the ground state a closed-shell singlet. Our previous theoretical study indicates that this is actually the case for $(CH_4)RhCl(PH_3)_2$.[9f]

The transition state shown in Figure 4 is tight and three-centered; the Rh–C bonds to be broken are slightly longer than those in the reactants, and the C–C bond of 1.972 Å is only 1.3 times longer than that in the product. The transition state is late as well; the Rh–CH_2(···CH_3) bond distance of 2.070 Å at the transition state is closer to the Rh–CH_2CH_3 distance of 4 than to the Rh–CH_2 distance of 3. The LMO for the Rh–CH_2(···CH_3) bond shown in Figure 2e resembles that for the Rh–CH_2CH_3 bond of the product shown in Figure 2c, indicating that the strain is already substantially released at the transition state. The structure of the rest of the molecule does not change very much.

The LMOs representing the interaction among two C atoms and Rh^1 at the transition state are shown in Figure 6b. They are the partially formed σ_{CC} bond and the d lone pair, which are slightly delocalized to the Rh dsp hybrid and σ_{CC}*, respectively. They respectively demonstrate donation and back-donation responsible for bond exchange in the oxidative addition, the reverse reaction of the present reductive elimination. It is noted that a different perspective of the same three-centered interaction can be obtained from the 1:1 linear combinations of these LMOs:

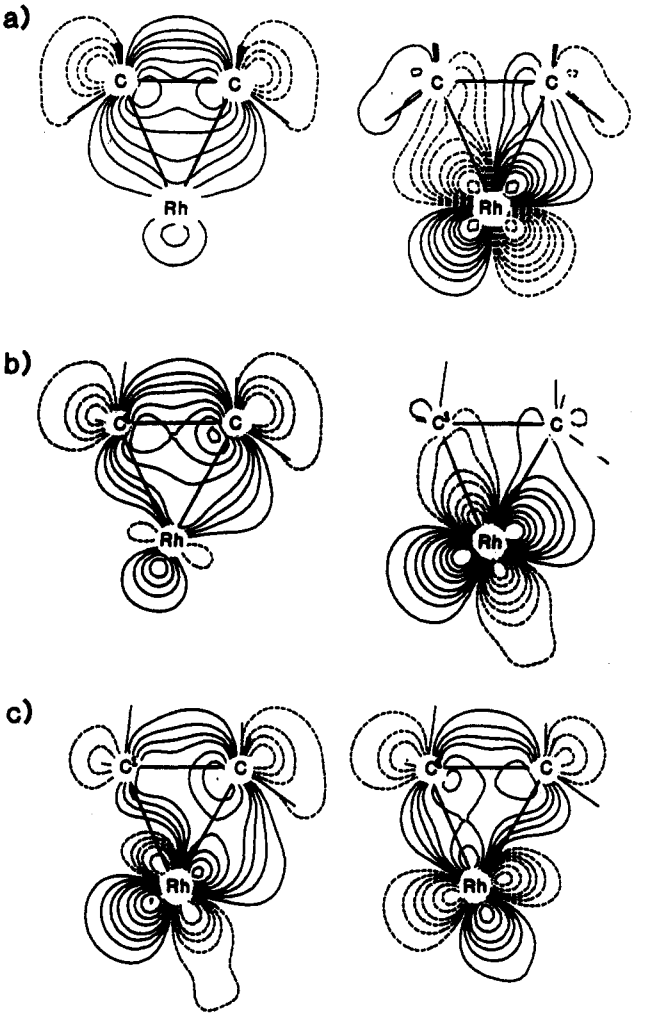

Figure 6. Boys-localized molecular orbitals at the three-centered transition state for (a) reductive elimination of $CpRh(PH_3)(CH_3)_2$, (b) CC coupling reaction of $(CpRh)_2(\mu\text{-}CH_2)_2(CH_3)(H)$, and (c) 1:1 linear combinations of LMOs shown in (b). The contours are ±0.3, ±0.25, ±0.2, ±0.15, ±0.1, ±0.075, ±0.05, and ±0.025 au, and solid and dotted lines denote positive and negative values, respectively.

two three-center two-electron C–C–Rh bonds, as shown in Figure 6c, which represent an intermediate stage of bond exchange in the reductive elimination.

The energy calculations with several basis sets at these optimized structures are shown in Table I. The energetics at the RHF level is not very dependent on the basis sets; the activation barrier ranges between 20 and 30 kcal/mol, and the exothermicity, between 4 and 15 kcal/mol. This shows again that the smallest basis function of STO-2G for ligands fortunately gives a good model of this reaction. On the other hand, the electron correlation changes the energetics substantially, making the reaction 34 kcal/mol more endothermic and the activation barrier 20 kcal/mol higher. This is what is expected qualitatively; the electron correlation would stabilize the reactant more than the product, when the bonds to be broken such as the Rh–C bonds are covalent with a large d character.[9f]

We also considered another possibility of the CC coupling reaction, an intramolecular dinuclear replacement mechanism, shown in eq 4.

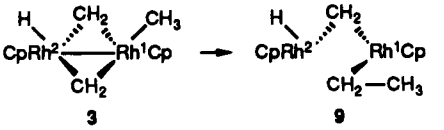

(4)

(22) Brookhart, M.; Green, M. L. H.; Wong, L.-T. *Prog. Inorg. Chem.* **1988**, *36*, 1 and references cited therein.

(23) (a) Cotton, F. A.; Jeremic, M.; Shaver, A. *Inorg. Chim. Acta* **1972**, *6*, 543. (b) Cotton, F. A.; LaCour, T.; Stanislowski, A. G. *J. Am. Chem. Soc.* **1974**, *96*, 754. (c) Cotton, F. A.; Day, V. W. *J. Chem. Soc., Chem. Commun.* **1974**, 415.

(24) (a) Koga, N.; Obara, S.; Morokuma, K. *J. Am. Chem. Soc.* **1984**, *106*, 4625. (b) Obara, S.; Koga, N.; Morokuma, K. *J. Organomet. Chem.* **1984**, *270*, C33. (c) Koga, N.; Morokuma, K. *J. Am. Chem. Soc.* **1988**, *110*, 108.

(25) (a) Jeffery, J. C.; Orpen, A. G.; Robinson, W. T.; Stone, F. G. A.; Went, M. J. *J. Chem. Soc., Chem. Commun.* **1984**, 396. (b) Davies, D. L.; Gracey, B. P.; Guerchais, V.; Knox, S. A. R.; Orpen, A. G. *J. Chem. Soc., Chem. Commun.* **1984**, 841.

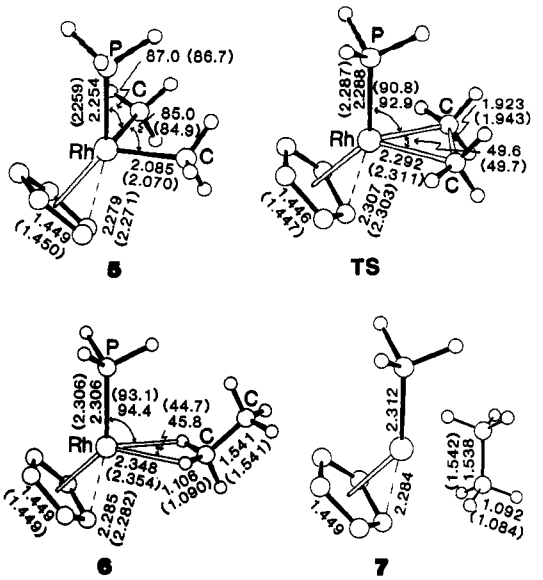

Figure 7. RHF/I-optimized structures in angstroms and degrees of $CpRh(PH_3)(CH_3)_2$ (**5**), $CpRh(PH_3)(C_2H_6)$ (**6**), the transition state between them, and $CpRh(PH_3)$ (**7**) with the constraint of an overall C_s symmetry and a local C_{5v} symmetry for Cp. The numbers in parentheses are those optimized with the basis set II. Hydrogen atoms of Cp's are omitted for clarity.

Table II. Energies (in kcal/mol) for the Reaction $CpRh(PH_3)(CH_3)_2 \rightarrow CpRh(PH_3) + C_2H_6$, Relative to the Reactant and Calculated for the RHF/I-Optimized Structures

method	reactant[a]	transition state	C_2H_6 complex	products
RHF/I	-611.9721	56.4	0.8	7.5
	(-611.9739)[b]	(54.1)	(-1.7)	(5.1)
RHF/II	-614.7252	61.6	11.3	15.0
	(-614.7257)[c]	(60.9)	(11.1)	(15.1)
RHF/III	-630.0141	58.7	3.8	6.1
RMP2/III	-630.8317	65.6	35.1	49.5
RHF/IV	-701.2282	55.3	2.5	5.1

[a] Total energies in hartree. [b] Calculated for the structures optimized without the C_{5v} constraint for Cp. [c] Calculated for the structures optimized with the basis set II.

In eq 4 the replacement of Rh^2 by CH_3 on μ-CH_2 takes place in which one Rh–ligand bond for each Rh atom as well as the Rh–Rh bond is lost. The Rh atoms in **9** have a formal electron count of d^6.

The geometry optimization of the replacement product, **9**, however, gave only **4**, the product of the reductive elimination; the ethyl group was transferred from Rh^1 to Rh^2 during optimization, suggesting that **9** is very unstable and that only the reductive elimination takes place. In **9**, two Rh atoms have the formal electron count of d^6 and a closed-shell electronic structure with a vacant coordination site like d^6 ML_5, suggesting the possibility of a Rh^1 occupied d → Rh^2 vacant d (or vice versa) dative bond. The calculated result that **9** is unstable relative to **4**, however, suggests that the interaction between the ethyl group and Rh^2 vacant d orbital is stronger than this dative bond.

Reductive Elimination of the Rh Mononuclear Complex. For the reductive elimination (eq 3) of a mononuclear complex the RHF/I-optimized structures of the reactant, **5**, the transition state, the C_2H_6 complex, **6**, and the products, **7**, are shown in Figure 7, together with the parameters optimized with the basis set II. The energetics is shown in Table II. The RHF/I structures are very similar to the RHF/II structures. The RHF/I geometry optimization again gives a proper structure model, probably because of cancellations of errors.

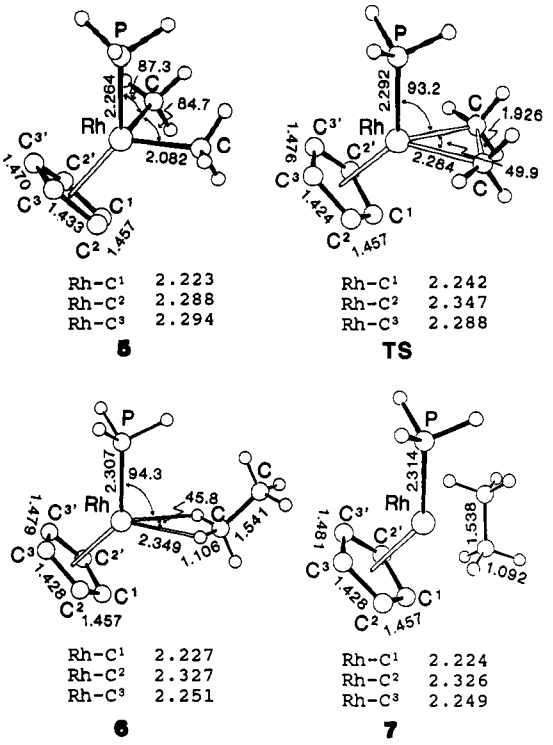

Figure 8. RHF/I-optimized structures in angstroms and degrees of $CpRh(PH_3)(CH_3)_2$ (**5**), $CpRh(PH_3)(C_2H_6)$ (**6**), the transition state between them, and $CpRh(PH_3)$ (**7**) with an overall C_s symmetry constraint but without a local C_{5v} symmetry for Cp.

The $Rh–CH_3$ bond (2.085 Å) of the reactant without strain is longer than the $Rh–CH_2$ bond (2.016 Å) of the dinuclear complexes, similar to the difference in the CC bond distance between ethane and cyclopropane mentioned above. The angles between the Rh–P and Rh–C bonds (87.0 and 85.0°) are close to 90°, indicating that $CpRh(PH_3)(CH_3)_2$ is electronically similar to the octahedral ML^6 with the formal electron count of d_6 (one can replace Cp^- by three CO ligands as mentioned above).

The transition state is three-centered, as expected for the reductive elimination,[9a,12] in which the Rh–C bonds to be broken (2.292 Å) are only 10% longer than those in the reactant, and thus one can say that this transition-state structure is earlier than that of the dinuclear complex in the preceding section. In this transition-state determination, we assumed the C_s symmetry with the eclipsed conformation of "ethane". The relaxation of this constraint would give the less hindered staggered conformation. The energy lowering due to the relaxation, however, would be a few kcal/mol. We did not determine the staggered transition state, since the main purpose here is the comparison of the reactions between dinuclear and mononuclear complexes and the difference in energetics between them is much larger than the difference between the staggered and the eclipsed conformations.

The LMOs representing the three-centered interaction among the Rh and the two carbons are shown in Figure 6a. They are very similar to those for the reaction of the Rh dinuclear complex and correspond to donation and back-donation.

In determining the structure of the C_2H_6 complex, we assumed the C_s symmetry with the two carbons of C_2H_6 on the symmetry plane, resulting in the bifurcated structure, in which two CH bonds interact with the Rh atom simultaneously. Such a bifurcated structure is the most stable among several possible structues for $(CH_4)RhCl(PH_3)_2$.[9f]

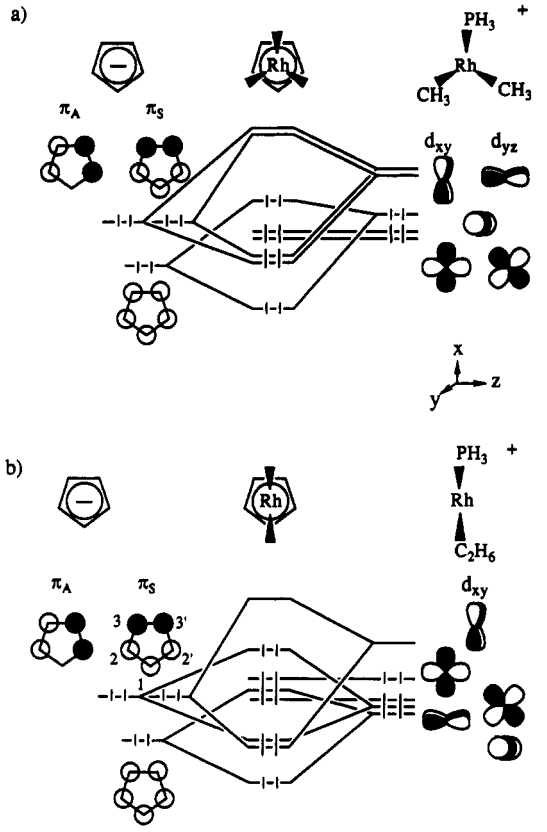

Figure 9. Schematic orbital interaction diagram for (a) d^6 $CpRh(PH_3)(CH_3)_2$ and (b) d^8 $CpM(PH_3)(C_2H_6)$.

In Figure 8, the structures optimized by using the basis set I without the restriction of local C_{5v} symmetry for the Cp ring are shown. In a d^6 complex, two π orbitals (π_A and π_S) of Cp interact with two vacant d orbitals (d_{xy} and d_{yz}) more or less equivalently, as shown in Figure 9a, and thus the local C_{5v} symmetry restriction for the reactant **5** is not bad. However, in a d^8 complex only one of d orbitals (d_{xy}) is vacant and accepts electrons from π_S, as shown for the C_2H_6 complex, **6**, in Figure 9b, leading to the weaker C^1–C^2 and C^3–$C^{3'}$ bonds and the stronger C^2–C^3 bonds. This also is the situation for both **7** and the transition state. The difference between the shortest and the longest Cp C–C bond lengths in **6** (0.051 Å) is larger than that in **5** (0.037 Å). The symmetry restriction for the Cp ring thus biases against the product. However, the energy lowering of the product due to the relaxation is only 2.4 kcal/mol relative to the reactant (Table II). Therefore, the C_{5v} restriction does not cause a serious problem in the present study.

Comparison of the CC Coupling Reaction with Reductive Elimination of the Mononuclear Complex. The three-centered transition-state structures for reactions 2 and 3 (Figures 4 and 7) are very similar to each other, although the one for the reaction 2 is located slightly earlier than that of the reaction 3; the Rh–C distances (2.159 and 2.269 Å) for reaction 2 are shorter than those (2.292 Å) for reaction 3, and the C–C distance (1.972 Å) for reaction 2 is longer than that (1.923 Å) for reaction 3. The LMOs calculated at the transition states shown in Figure 6 are very similar to each other as well. These similarities also support that the CC coupling reaction of this dinuclear complex is a simple reductive elimination.

The energetics of reaction 3 is, however, different from that of reaction 2; the activation barrier is higher and the reaction is more endothermic. At the RMP2/III level, the differences in the activation energy and the energy of reaction are 23.8 and 10.2 kcal/mol, respectively. For the latter the energy of the C_2H_6 complex is compared with that of the product for the reaction 2, since both have a CH···Rh interaction. A high activation barrier has been calculated previously for the reductive elimination in which two alkyl groups form a CC bond.[12] The directionality of the sp^3 lobe orbitals has been ascribed to this high activation barrier.

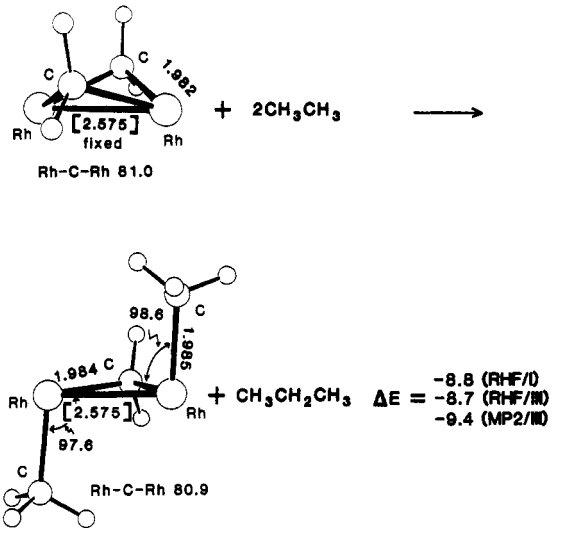

Figure 10. RHF/I-optimized structures in angstroms and degrees of $Rh_2(\mu\text{-}CH_2)_2$ and $Rh_2(\mu\text{-}CH_2)(CH_3)_2$ with the relative energies in kcal/mol at the RHF/I, the RHF/III, and the RMP2/III levels.

The lower activation barrier of reaction 2 is, therefore, considered to originate from the fact that the system is dinuclear. A possible origin is the strain in the reactant, as we discussed above. The strain in the $RhCH_2Rh$ triangle is released during the reaction, which would make the reaction more exothermic and thus lower the barrier.

In order to analyze the strain more quantitatively, we considered isodesmic reaction 5. There are four strained

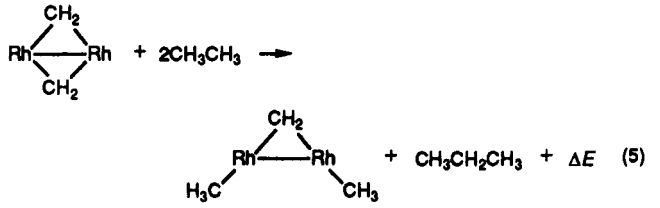

$Rh–CH_2$ bonds, one Rh–Rh σ bond, and two normal C–C bonds on the left-hand side of eq 5 and two unstrained Rh-C bonds, two strained $Rh–CH_2$ bonds, one Rh–Rh σ bond and two normal C–C bonds on the right. Therefore, ΔE would give the strain in a $RhCH_2Rh$ ring.

The structures of $Rh_2(\mu\text{-}CH_2)_2$ and $(RhCH_3)_2(\mu\text{-}CH_2)$ as well as ethane and propane were optimized with the basis set I, and ΔE was calculated with the basis set III at the RMP2 level. To simulate the strain in **3**, however, the Rh–Rh distance was fixed to that of **3** (2.575 Å). Their structures and ΔE calculated values are shown in Figure 10. As expected, we found a large $RhCH_2Rh$ ring strain of 9.4 kcal/mol at the RMP2/III level. This is very close to the difference (10.2 kcal/mol) in the energy of reaction between the mononuclear and the dinuclear complexes, supporting the above discussion.

The difference in the activation barriers between two reactions is larger than that of endothermicity by 14 kcal/mol at the RMP2/III levels; the dinuclear complex is more reactive than expected from the endothermicity. This further enhancement of reactivity may be ascribed to the electronic characteristics of the strained $Rh–CH_2$

Table III. Changes of the Mulliken Net Charges of the Eliminating Groups in the Reactions $(CpRh)_2(\mu\text{-}CH_2)_2(CH_3)(H) \rightarrow (CpRh)_2(\mu\text{-}CH_2)(C_2H_5)(H)$ and $CpRh(PH_3)(CH_3)_2 \rightarrow CpRh(PH_3) + (C_2H_6)$[a]

	reactant	transition state	product
	$CpRh(PH_3)(CH_3)_2$ (5)		
CH_3	−0.1597	0.0077	0.0
	$(CpRh)_2(\mu\text{-}CH_2)_2(CH_3)(H)$ (3)		
CH_3	−0.1058	−0.0452	0.0320
CH_2	0.0555	0.0811	−0.0521

[a] Calculated at the RHF/III level.

bonds. In the third section, we have noticed that the Rh–CH_2 bond is less polarized than the Rh–CH_3 bond. The Mulliken population analysis, shown in Table III, shows that negative charge on the CH_3 group of **5** decreases during the reaction, corresponding to the reductive process. Similarly, the CH_3 group in **3** loses the negative charge. On the other hand, the μ-CH_2 group of **3** has a small positive charge and becomes slightly negative in the product, **4**, where CH_2 is a part of the ethyl ligand having a negative charge. The more positive charge on μ-CH_2 than CH_3, which is due to the strain, suggests that the Rh atom in **3** is already partially "reduced". In addition, electrostatically the interaction between CH_3 and the positive μ-CH_2 in **3** should be more favorable than that between the two negative CH_3 groups in **5**.

Recently, we have proposed a simple scheme for changing the Coulomb integral arbitrary within the ab initio MO methods by using the shift operator.[26] The shift operator, $B|\phi\rangle\langle\phi|$, changes the electronegativity of a ligand without introducing substituents. Here, we placed such a shift operator with the shift parameter B of +0.3 hartree and with the hydrogen 1s orbital as ϕ on the hydrogens of one of the CH_3 ligands of **5** and the transition state for the reaction of **5**. This means that the hydrogen 1s orbitals of this CH_3 ligand are shifted up by 0.3 hartree in energy and thus they become more electropositive. Consequently, one could know how the activation energy changes, when one of the CH_3 ligands of **5** is more electropositive. The calculations were carried out at the RHF/I optimized structures shown in Figure 7, which were determined with the normal CH_3 ligand. At the RHF/III level the Mulliken net charge of this electropositive CH_3 ligand in "**5**" is 0.0659, comparable with that of μ-CH_2 in **3**. The shift operators lower the activation energies of **5** by 14.2, 20.0, and 11.6 kcal/mol at the RHF/I, RHF/III, and RMP2/III levels, respectively,[27] suggesting that the larger electropositivity of μ-CH_2, relative to CH_3, due to the strain, is the additional factor that lowers the barrier.

Therefore, one can conclude that the reductive elimination of CH_3 and μ-CH_2 ligands in **3** is favored thermodynamically by the releasing of the strain as well as by the effect of the electropositive μ-CH_2 ligand lowering the activation barrier. This result also suggests a high reactivity of the bridged methylene appearing in Scheme I, a mechanism of Fischer–Tropsch synthesis.

Concluding Remarks

We studied the structure of $(CpRh)_2(\mu\text{-}CH_2)_2(CH_3)_2$ and the CC coupling reaction of $(CpRh)_2(\mu\text{-}CH_2)_2(CH_3)(H)$ by the ab initio MO method. The structures of these dinuclear complexes, the product, and the transition state of the reaction were determined at the RHF level. The calculated structure of $(CpRh)_2(\mu\text{-}CH_2)_2(CH_3)_2$ is very similar to the X-ray structure of $(Cp^*Rh)_2(\mu\text{-}CH_2)_2(CH_3)_2$. The localized orbital analysis clearly showed the existence of the Rh d–Rh d σ bond and strained Rh–(μ-CH_2) σ bonds. The CC coupling reaction is a reductive elimination with the activation barrier of 42 kcal/mol and the endothermicity of 25 kcal/mol at the RMP2 level. These values are smaller than those for the reductive elimination of mononuclear complex $CpRh(PH_3)(CH_3)_2$. The higher reactivity of μ-CH_2, relative to the terminal CH_3, is ascribed in part to a strain in the $RhCH_2Rh$ triangle, which was estimated to be 9 kcal/mol at the RMP2 level by using an isodesmic reaction. Further, we have found that μ-CH_2 is more electropositive than the terminal CH_3 because of the strain and that this lowers the activation barrier. No

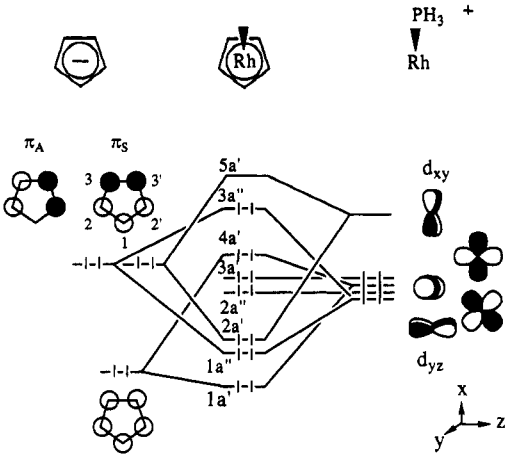

Figure 11. Schematic orbital interaction diagram for $CpRh(PH_3)$.

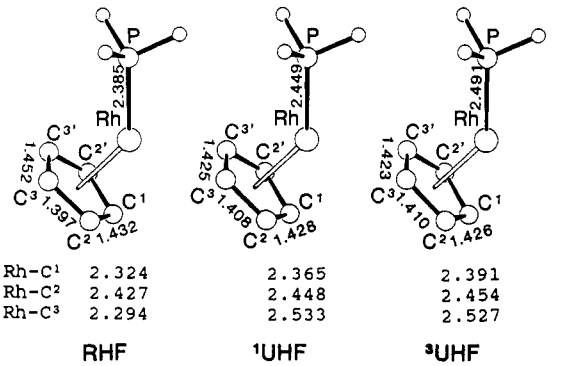

Figure 12. Optimized structures in angstroms for $CpRh(PH_3)$ with RHF, singlet UHF, and triplet UHF methods.

Table IV. Relative Energies in kcal/mol of $CpRh(PH_3)$ for Three Lower States[a]

		open-shell singlet		
method	closed-shell singlet R[b]	U[c]	APU[d] (SPU)[e]	triplet U[c] (SPU)[e]
HF	31.8	17.4	35.0 (27.2)	0.0 (0.0)
MP2	11.5	12.0	26.1 (21.2)	0.0 (0.0)
MP3	18.0	13.3	28.3 (22.8)	0.0 (0.0)
MP4SDQ	11.3	11.4	24.5	0.0
MP4SDTQ	7.8	10.5	22.5	0.0

[a] At the optimized structures of Figure 12. [b] Restricted. [c] Unrestricted. [d] Approximately projected unrestricted.[32] Only the unrestricted triplet state is projected out. [e] Projected unrestricted by means of Schlegel's method.[33] Only the triplet state is projected out from the singlet unrestricted and the quintet state from the triplet unrestricted.

(26) Koga, N.; Morokuma, K. *Chem. Phys. Lett.* **1990**, *172*, 243.
(27) Effects of the electronegativity of the eliminating groups have been taken into account by extended Hückel calculations[27a] for the group 10 transition-metal complexes, and it has been found that the σ-donating eliminating group favors the reductive elimination: Tatsumi, K.; Hoffman, R.; Yamamoto, A.; Stille, J. K. *Bull. Chem. Soc. Jpn.* **1981**, *54*, 1857.

path of CC coupling via an intramolecular dinuclear replacement reaction has been found.

Acknowledgment. We acknowledge Prof. K. Isobe for valuable discussions. All the calculations were carried out at the Computer Center of IMS.

Appendix

Electronic Structure of $CpRh(PH_3)$. The ground state of CpML with the formal electron count of d^8 has so far been discussed by the extended Hückel method,[28a,b] the ab initio SCF method,[28b] and the density functional.[28c] Its d levels are schematically shown in Figure 11. Since 3a″ and 5a′ are close in energy, one anticipates three low-dying electronic states: a closed shell singlet $(3a'')^2$, an open-shell singlet, and a triplet $(3a'')^1(5a')^1$. We optimized the structure of $CpRh(PH_3)$ with the RHF and the singlet and triplet UHF methods, as shown in Figure 12, under the constraint of C_s symmetry with the nine valence electron ECP and the DZ basis functions for Rh[14a] and the 3-21G for Cp and PH_3.[15b,29]

In the RHF-optimized structure, two C^2–C^3 bonds of the Cp ring are much shorter than the other C–C bonds. In the closed-shell singlet state, the antibonding 3a″ is doubly occupied and thus the Cp π_A orbital does not contribute to the RhCp bonding interaction. Only the electron donation from π_S to d_{xy} is responsible for the RhCp bonding interaction. Therefore, representing the bond order in π_S, the C^2–C^3 bonds are shorter than the C^1–C^2 and C^3–$C^{3'}$ bonds.

In the open-shell states, on the other hand, 3a″ and 5a′ are singly occupied, and π_A and π_S interact with d_{yz} and d_{xy} equivalently. Therefore, the five CC distances in the Cp ring are close to each other.

In Table IV we show the relative energies calculated at the several levels with a larger basis set: [2s2p3d]/(3s3p4d) for Rh, [4s3p]/(11s8p) for P, [3s2p]/(8s5p) for C, and [2s]/(4s) for H.[14a,30,31] At all the levels of calculation, the triplet is the ground state of $CpRh(PH_3)$. At the highest level of calculation, MP4SDTQ, the closed-shell singlet is 8 kcal/mol higher in energy than the triplet. The open-shell singlet is the most unstable. These results are different from the density functional calculations,[28c] which gives the closed-shell singlet of CpML (M = Ir, Rh; L = CO, PH_3) as being more stable, than the triplet by 1–6 kcal/mol.

(28) (a) Hofmann, P.; Radmanabhan, M. *Organometallics* **1983**, *2*, 1273. (b) Veillard, A.; Dedieu, A. *Theor. Chim. Acta* **1980**, *63*, 339. (c) Ziegler, T.; Tschinke, V.; Fan, L.; Becke, A. D. *J. Am. Chem. Soc.* **1989**, *111*, 9177.

(29) Gordon, M. S.; Binkley, J. S.; Pople, J. A.; Pietro, W. J.; Hehre, W. J. *J. Am. Chem. Soc.* **1982**, *104*, 2797.

(30) Huzinaga, S.; Andzelm, J.; Kłobukowski, M.; Radzio-Andzelm, E.; Sakai, Y.; Tatewaki, H. *Gaussian basis sets for molecular calculations*; Elsevier: Amsterdam, 1984.

(31) Dunning, T. H. *J. Chem. Phys.* **1970**, *53*, 2823.

(32) Yamaguchi, K.; Takahara, Y.; Fueno, T.; Houk, K. N. *Theor. Chim. Acta* **1988**, *73*, 337.

(33) Schlegel, H. B. *J. Chem. Phys.* **1986**, *84*, 4530.

Synthesis and Photochemical Reactivity of Transition-Metal-Disubstituted Disilanes $LMSiMe_2SiMe_2ML$ (LM = $(\eta^5\text{-}C_5H_5)Fe(CO)_2$ and $(\eta^5\text{-}C_5H_5)Fe(\eta^5\text{-}C_5H_4)$)[1]

Keith H. Pannell* and Hemant Sharma

Department of Chemistry, The University of Texas at El Paso, El Paso, Texas 79968-0513

Received June 27, 1990

Three transition-metal-disubstituted disilanes, $[(\eta^5\text{-}C_5H_5)Fe(CO)_2]_2SiMe_2SiMe_2$ ($FpSiMe_2SiMe_2Fp$, I), $[(\eta^5\text{-}C_5H_5)Fe(\eta^5\text{-}C_5H_4)]_2SiMe_2SiMe_2$ ($FcSiMe_2SiMe_2Fc$, II), and $FpSiMe_2SiMe_2Fc$ (III), have been synthesized, characterized, and studied photochemically. Complex I undergoes rearrangement to $(\eta^5\text{-}C_5H_5)_2Fe_2(CO)_2(\mu\text{-}CO)(\mu\text{-}SiMeSiMe_3)$ (IV) as well as smaller amounts of $FpSiMe_3$. Complex II is photochemically inert in nonpolar solvents but undergoes an oxidative methanolysis reaction in MeOH in the presence of O_2 to form $FcSiMe_2OMe$ (V) as the only product. Complex III, which contains the activating Fp group and the deactivating Fc group, reacts photochemically to form $FpSiMe_2Fc$ (VI) and $FpSiMe_3$ in the ratio 3:1. Photolysis of $FpSiMe_2SiMe_2Cl$ was also performed and produced $FpSiMe_2Cl$ and $FpSiMe_3$ in the ratio 4:1. The various results illustrate that loss of $SiMe_2$ is much favored compared to loss of SiMeR, R = Ph, Cl, and Fc, where competition is possible. The various ferrocenylsilanes were prepared from the appropriate chlorosilanes and Fc^-Li^+ prepared from the transmetalation reaction between (chloromercurio)ferrocene and *n*-butyllithium. The yields, in the 70% range, were far superior to published values of approximately 10% obtained by using Fc^-Li^+ prepared directly from ferrocene.

Introduction

The photochemical properties of oligo- and polysilanes have been well studied, and in particular the photochemistry of aryldisilanes and related compounds has been an area of active research.[2] In general, such photolyses are thought to involve an excited state that leads to cleavage of the Si–Si bond to form the corresponding silyl radicals, which may either recombine or be trapped by appropriate agents. We have an ongoing interest in the chemical and

(1) Organometalloidal Derivatives of the Transition Metals. 26. Part 25: Pannell, K. H.; Lin, H.-S.; Kapoor, R. N.; Cervantes-Lee, F.; Pinon, M.; Parkanyi, L. *Organometallics* **1990**, *9*, 2454.

(2) (a) For a review of the area, see: Ishikawa, M.; Kumada, M. *Advances In Organometallic Chemistry*; Ed. F. G. A., Stone, R., West, Eds.; Academic Press: New York, 1981; Vol. 19, p 51. (b) For a recent article concerning related photochemical studies, see: Hu, S-S.; Weber, W. F. *J. Organomet. Chem.* **1989**, *369*, 155.

0276-7333/91/2310-0954$02.50/0